molecular pharmaceutics

Article

pubs.acs.org/molecularpharmaceutics

Effective Elimination of Cancer Stem Cells by Magnetic Hyperthermia

Tanmoy Sadhukha,[†] Lin Niu,[†] Timothy Scott Wiedmann,[†] and Jayanth Panyam*[,†,‡]

[†]Department of Pharmaceutics, College of Pharmacy, University of Minnesota, Minneapolis, Minnesota 55455, United States

[‡]Masonic Cancer Center, University of Minnesota, Minneapolis, Minnesota 55455, United States

Supporting Information

ABSTRACT: Cancer stem cells (CSCs) are a subpopulation of cancer cells that have stem cell-like properties and are thought to be responsible for tumor drug resistance and relapse. Therapies that can effectively eliminate CSCs will, therefore, likely inhibit tumor recurrence. The objective of our study was to determine the susceptibility of CSCs to magnetic hyperthermia, a treatment that utilizes superparamagnetic iron oxide nanoparticles placed in an alternating magnetic field to generate localized heat and achieve selective tumor cell kill. SPIO NPs having a magnetite core of 12 nm were used to induce magnetic hyperthermia in A549 and MDA-MB-231 tumor cells. Multiple assays for CSCs, including side population phenotype, aldehyde dehydrogenase expression, mammosphere formation, and *in vivo* xenotransplantation, indicated that magnetic hyperthermia reduced or, in some cases, eliminated the CSC subpopulation in treated cells. Interestingly, conventional hyperthermia, induced by subjecting cells to elevated temperature (46 °C) in a water bath, was not effective in eliminating CSCs. Our studies show that magnetic hyperthermia has pleiotropic effects, inducing acute necrosis in some cells while stimulating reactive oxygen species generation and slower cell kill in others. These results suggest the potential for lower rates of tumor recurrence after magnetic hyperthermia compared to conventional cancer therapies.

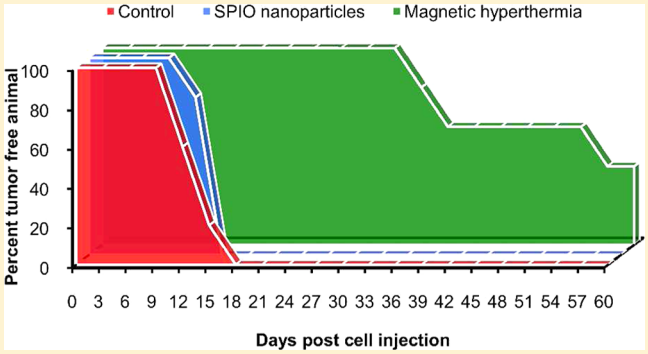

KEYWORDS: *superparamagnetic iron oxide, magnetic hyperthermia, cancer stem cells, necrosis, reactive oxygen species, mammosphere, clonogenicity, tumorigenicity, aldehyde dehydrogenase*

INTRODUCTION

A number of recent studies suggest that tumors consist of a minor population of stem-like cells (cancer stem cells; CSCs) that are capable of generating and maintaining a tumor in its entirety.[1] These cells have the capacity for asymmetric cell division, generating one identical daughter cell and another that is committed to a distinct differentiation pattern. The latter undergoes a series of divisions and differentiation steps that result in the generation of terminally differentiated cell populations. Cells in the intermediate states are referred to as progenitors, transit cells, or transit amplifying cells.[2] All of these phenotypes, collectively termed tumor-initiating cells, have the potential to give rise to a complete tumor. CSCs are resistant to conventional chemotherapy and can initiate tumor recurrence following treatment.[3] CSCs possess several defense mechanisms including overexpression of efflux pumps that can eliminate cytotoxic drugs,[4] increased expression of DNA-repair proteins that can counteract DNA damage,[5] elevated antioxidant concentrations to defend against reactive oxygen species (ROS),[6] and low rate of cell division.[7] Tumors can become enriched in CSCs after conventional treatments,[5,8] which could account for frequent tumor relapse observed in many cancers.

Hyperthermia, which utilizes elevated temperatures in the range of 41−46 °C to kill tumor cells,[9] has been shown to improve treatment response and survival when used in combination with radiotherapy, surgery, and/or chemotherapy.[10,11] In mouse tumor models, the addition of local hyperthermia significantly increased the sensitivity of CSCs to radiotherapy.[12] Magnetic hyperthermia is a related approach that utilizes superparamagnetic iron oxide nanoparticles (SPIO NPs) placed in an alternating magnetic field to generate heat for a highly localized tumor cell kill.[13] Magnetic hyperthermia is currently in clinical trials in Europe for glioblastoma as well as prostate and pancreatic cancers.[14] While a number of previous studies have demonstrated the anticancer efficacy of magnetic hyperthermia,[15] the effect of magnetic hyperthermia on CSCs has not been reported to date. Using various *in vitro* and *in vivo* assays, we evaluated the ability of SPIO NP-mediated magnetic hyperthermia to effectively eliminate CSCs.

EXPERIMENTAL SECTION

Materials. Ferrous chloride tetrahydrate, ferric chloride hexahydrate, myristic acid, Pluronic F127, ascorbic acid,

Received: January 9, 2013
Revised: February 11, 2013
Accepted: February 22, 2013
Published: February 22, 2013

   dx.doi.org/10.1021/mp400015b | *Mol. Pharmaceutics* 2013, 10, 1432−1441

potassium hydroxide, 1,10-phenanthroline, and sodium acetate were purchased from Sigma (St. Louis, MO). Penicillin/streptomycin, fetal bovine serum (FBS), RPMI 1640, Dulbecco's phosphate-buffered saline (DPBS), F-12K (Kaighn's modification), MEM, nonessential amino acids, sodium pyruvate, and trypsin-ethylenediaminetetraacetic acid (EDTA) solution were obtained from Invitrogen Corporation (Carlsbad, CA). Cytotox 96 nonradioactive cytotoxicity assay kit was purchased from Promega (Madison, WI).

Methods. *Synthesis of Water-Dispersible SPIO NPs.* A stable aqueous dispersion of SPIO NPs was prepared from iron chlorides as previously described.[16] In brief, 0.82 g of ferric chloride hexahydrate and 0.33 g of ferrous chloride tetrahydrate were dissolved in 30 mL of degassed and nitrogen-purged water, and 3 mL of 5 M ammonium hydroxide was added dropwise to this solution and stirred for 30 min. Iron oxide nanoparticles formed were washed three times with nitrogen-purged water (each wash followed by magnetic separation of nanoparticles), sonicated in a water bath sonicator for 2 min, and heated to 80 °C. About 100 mg of myristic acid was added to the heated mixture and stirred for another 30 min. Particles were washed twice with acetone to remove excess myristic acid, followed by two additional washes with water to remove excess acetone. Myristic acid-coated particles were then suspended in 30 mL of water; 100 mg of pluronic F127 was added, and the mixture was stirred overnight. The final dispersion was lyophilized (Labconco, FreeZone 4.5, Kansas City, MO) to obtain SPIO NPs. Every step of the synthesis was carefully conducted to minimize exposure to atmospheric oxygen.

Characterization of SPIO NPs. Dynamic light scattering was used to determine the hydrodynamic diameter of SPIO NPs. About 0.5 mg/mL of SPIO NPs dispersed deionized water was subjected to particle size analysis using a Delsa Nano C Particle Analyzer (Beckman, Brea, CA). Transmission electron microscopy (TEM) of SPIO NPs was performed using a JEOL JEM-1210 transmission electron microscope (Peabody, MA). A drop of an aqueous dispersion of SPIO NPs was placed on a Lacey carbon-coated copper grid (300 mesh, Ted Pella Inc. Redding, CA) and allowed to air-dry before imaging. Diameters of 100 different particles were measured from different TEM images using ImageJ software. The average diameter along the horizontal axis was determined as the mean Feret's diameter. The mean crystallite size of SPIO NPs was calculated from their X-ray diffraction pattern. SPIO NPs were subjected to a Cu−Kα radiation (45 kV, 40 mA) in a wide-angle powder X-ray diffractometer (D5005, Siemens, Madison, WI). The instrument was operated in the step-scan mode in increments of 0.05° 2θ over an angular range of 10−100° 2θ with a dwell time of 1 s for each scan step. Data analysis was performed using OriginPro 8 software (OriginLab Corporation, Northampton, MA). Five highest peaks (at 30.1°, 35.5°, 43.1°, 57.1°, and 62.7° 2θ) were fit using the pseudo-Voigt profile function, which is a linear combination of the Gaussian and Lorentzian components of the diffraction peaks. The Scherrer equation was utilized to determine the mean particle size of SPIO NPs.[17]

Fourier-transformed infrared spectroscopy (FT-IR) of SPIO NPs was performed using Vertex 70 FT-IR spectrophotometer (Bruker Optics Inc., Billerica, MA). About 5 mg of SPIO NPs were added to the FT-IR stage and scanned from 4000 cm^{-1} to 400 cm^{-1}. Each spectrum was obtained as an average of 16 interferograms at a resolution of 2 cm^{-1} and analyzed using OPUS software (Bruker Optics Inc., Billerica, MA). Magnetic properties were determined using a vibrating sample magnetometer (Micromod model 3900, Princeton, NJ) operating at room temperature. Accurately weighed samples of SPIO NPs was sprinkled on a lightly greased silicon wafer and their magnetization curves were recorded in magnetic fields ranging from −1 to 1 T, at increments of 0.002 T. The saturation magnetization per gram of magnetite was calculated from the magnetization curves normalized to the weight of magnetite added. The composition of SPIO NPs was estimated using 1,10-phenanthroline-based iron assay.[18] About 5 mg of SPIO NPs was dissolved in 12 N hydrochloric acid and then diluted with distilled water to obtain a final acid concentration of 0.2 N. Samples of 10 mg/mL ascorbic acid, 22.4 mg/mL potassium hydroxide, 123 mg/mL sodium acetate, and 1.2 mg/mL 1,10-phenanthroline were added to the SPIO NP solution in a volume ratio of 1:1:5:1:1. The absorbance at 490 nm was recorded using a microplate reader (ELx800 Absorbance Microplate Reader, Biotek, Winooski, VT), and the iron content was analyzed using ferric chloride (hexahydrate) solutions in 0.2 N hydrochloric acid as a standard.

Magnetic Heating Rate. SPIO NPs were dispersed in 1 mL of Hank's F-12K medium or in 1 mL of molten 3% agarose, which was then allowed to form a gel in 10 mm × 75 mm disposable borosilicate glass cell culture tubes. Magnetic heating was performed using an induction heating system (1 kW Hotshot, Ameritherm Inc., Scottsville, NY) by placing the suspension at the center of a multiturn copper coil that generated the alternating magnetic field (nominal magnetic field strength of 6 kA/m and frequency of 386 kHz). The temperature change was measured using a fluoroptic probe (Lumasense Technologies, Santa Clara, CA). Samples were thermally equilibrated to 37 °C before exposure to the field.

Cell Culture Studies. A549 (human lung adenocarcinoma) and MDA-MB-231 (human mammary adenocarcinoma) cells were used in the study. A549 cells were propagated using F-12K medium supplemented with 10% fetal bovine serum (FBS) and 1% antibiotic solution. MDA-MB-231 cells were grown in MEM supplemented with 10% FBS, 1% nonessential amino acids, 1% sodium pyruvate, and 1% antibiotic solution. Both cell lines were maintained at 37 °C and in 5% carbon dioxide.

Effect of Magnetic Hyperthermia on CSCs. a. Side Population Determination. Following magnetic hyperthermia, A549 cells were centrifuged and resuspended in prewarmed 1 mL of Dulbecco's modified Eagle's medium (DMEM) with 2% FBS and 10 mM 4-(2-hydroxyethyl)-1-piperazineethanesulfonic acid (HEPES). Hoechst 33342 dye was added at a concentration of 5 μg/mL. In each treatment group, one sample was pretreated with 2 μM tariquidar, an inhibitor of Hoechst efflux. Cells were then incubated at 37 °C for 90 min with occasional shaking. Cells were then washed with chilled Hank's balanced salt solution (HBSS) with 2% FBS and 10 mM HEPES buffer and resuspended in chilled buffer. 7-A minoactinomycin-D (7AAD) was added to the sample tubes before flow cytometric analysis to gate for live cells. Flow analysis was carried out on a FACSDiva (BD Biosciences); Hoechst 33342 dye was excited at 357 nm, and the fluorescence was measured at 402−446 nm (blue) and 650−670 nm (red) wavelengths.[19,20]

b. Mammosphere Assay. Following magnetic hyperthermia, MDA-MB-231 cells were washed and resuspended in cell culture medium. About 3000 live cells (counted by trypan blue exclusion) were plated in ultralow adhesion 6-well plates with 2 mL of mammosphere formulation (DMEM/F-12 medium supplemented with 10 ng/mL human-fibroblast growth factor, 20 ng/mL recombinant human epidermal growth factor, 0.4%

bovine serum albumin, 5 μg/mL insulin, and 1% antibiotics). The number of mammospheres formed was counted under a light microscope 5 days after treatment.[21]

c. Aldehyde Dehydrogenase Assay. Thirty million MDA-MB-231 cells were sorted based on their levels of aldehyde dehydrogenase (ALDH) enzyme using the ALDEFLUOR kit (STEMCELL Technologies Inc., Vancouver, Canada).[22] Prior to sorting, 5 μL of the activated reagent was added to each milliliter of the cell suspension (1 million cells/mL), mixed well, and 500 μL of the suspension was immediately transferred to another tube containing 5 μL of diethylaminobenzaldehyde (DEAB) reagent in 95% ethanol. The tubes were incubated for 45 min at 37 °C, following which the cells were centrifuged in cold, and redispersed in cold ALDEFLUOR assay buffer and stored on ice. Cells were then sorted using BD FACSVantage (BD Biosciences) cell sorter. Cells incubated with DEAB reagent were used to gate for cells having low ALDH level ($ALDH_{low}$), and cells to the right of the gate were sorted as $ALDH_{high}$ population. Around 3−4% of MDA-MB-231 cells were $ALDH_{high}$. ALDH-sorted cells were subjected to 30 min of magnetic hyperthermia. Cells incubated with or without SPIO NP and not exposed to alternating magnetic field were used as controls. Treated cells were evaluated for clonogenicty as described above.

d. Tumorigenicity Assay. The study was carried out in compliance with protocol approved by the Institutional Animal Care and Use Committee at the University of Minnesota. Female BALB/c-nude mice (C.Cg/AnNTac-Foxn1^{nu} NE9; Taconic Farms), four to six weeks of age, were used for the studies. Mice received either 5000 or 50 000 live A549 cells (viability determined through trypan blue exclusion) that were previously subjected to 30 min of magnetic hyperthermia. Animals that received similar number of untreated cells or cells treated with SPIO NPs but not exposed to alternating magnetic field served as controls. Animals were observed once every three days for the appearance of palpable tumors.[19] Tumor dimensions were also measured using a digital calipers, and the tumor volume (V) was calculated using the formula $V = 0.5(L \times W^2)$, where L and W are the longest and shortest diameters, respectively. The development of 100 mm^3 tumors or 60 days after cell injection (whichever came first) marked the end of the study for each animal.

Cytotoxicity Studies. a. Cell Death after Magnetic Hyperthermia. About 1 million cells were suspended in 500 μL of RPMI (without phenol red and with 5% FBS). 500 μL of 5 mg/mL SPIO NP dispersion in the same medium was added to the cell suspension placed in an alternating magnetic field (6 kA/m, 386 kHz) for 5, 15, or 30 min. The cell suspension temperature was carefully maintained between 43 and 46 °C (Supporting Information, Figure 1). Cells with or without SPIO NPs and not exposed to alternating magnetic field were used as controls. In addition, cells incubated in a water bath at 46 °C for 30 min, with or without SPIO NPs, served as conventional hyperthermia controls. Following treatment (after 2 h), the cells were pelleted down, and the amount of lactate dehydrogenase (LDH) released by the cells in the supernatant was analyzed. LDH released by the untreated control was used to normalize for the background cell death, and LDH released by equal number of freeze−thaw lysed cells was used to calculate 100% cell death.

To evaluate the induction of apoptosis by magnetic hyperthermia, treated cells were gently dispersed in medium containing 10% FBS and plated in 6-well plates. After another 10 h, A549 cells were examined for apoptosis/necrosis by a flow-cytometry-based annexin-V fluorescein isothiocyanate (FITC)/propidium iodide (PI) assay. Briefly, cells were trypsinized and then centrifuged at 1000 rpm for 8 min. The cell pellets were stained with FITC-conjugated annexin-V and PI according to manufacturer's instructions (BD Pharmingen, San Jose, CA) and then immediately analyzed using a flow cytometer (BD FACSCalibur, BD Biosciences, San Jose, CA). FITC and PI fluorescence emissions were detected in FL-1 (515−545 nm) and FL-3 (670 long-pass) modes, respectively. Data from at least 10 000 cells were analyzed using Cyflogic software (Cyflo Ltd., Turku, Finland).

b. Clonogenicity. Clonogenicity was used as a measure of the proliferative potential of cells subjected to magnetic hyperthermia.[23] Following treatment, 200 live cells (identified by trypan blue exclusion assay) from each group were plated in a 10 cm culture dish and allowed to form colonies. After 2 weeks (about 12−15 cell doubling times[24,25]), the plates were washed with DPBS and fixed with 5% formalin in DPBS for 3 min. Colonies were further washed with DPBS and then stained with 0.05% crystal violet for 30 min. Plates were then washed gently with water and air-dried, and the number of colonies formed in each treatment groups was counted. Colonies were counted prior to and after washing and staining steps to account for the loss of colonies during the processing steps.

c. Instantaneous Cell Death during Magnetic Hyperthermia. Following incubation of A549 cells with SPIO NPs, 2 mM 7AAD, a cell viability stain, was added to the cells prior to exposing them to magnetic field. Cells not exposed to alternating magnetic field, with or without SPIO NPs, and cells exposed to 30 min of conventional hyperthermia were used as controls. Following treatments, cells were immediately washed by centrifugation, resuspended in RPMI (without phenol red) and subjected to flow cytometry. 7AAD fluorescence was detected in the FL-3 channel. Data from 20 000 cells in each group were analyzed using Cyflogic software.

Reactive Oxygen Species (ROS) Generation after Magnetic Hyperthermia. Immediately prior to magnetic hyperthermia treatment, 5-(and-6)-chloromethyl-2′,7′-dichlorodihydrofluorescein diacetate, acetyl ester (CM-H_2DCFDA) (7.5 μM) and PI (10 μM) were added to A549 cell suspension. Cells were subjected to magnetic hyperthermia and then to flow cytometric analysis. The deacetylated and oxidized product, 2′,7′-dichlorofluorescein, formed due to ROS generation in the cells, was detected in the FL-1 channel while PI fluorescence was detected in the FL-3 channel.

To determine the role of ROS in inducing cell death, cells were pretreated with 10 mM *N*-acetyl cysteine for 1 h before adding CM-H_2DCFDA and then subjected to 5 min of magnetic hyperthermia. Cells treated with 5 mM hydrogen peroxide with and without *N*-acetyl cysteine pretreatment served as additional controls.

Statistical Analysis. Statistical analyses were performed using one-way analysis of variance (ANOVA) by the Bonferroni-Holm method for comparison between individual groups. A probability level of $P < 0.05$ was considered significant.

RESULTS

Characterization of SPIO NPs. The physicochemical properties of SPIO NPs used in this study are summarized in Table 1. The particles were composed of 74 ± 2% (w/w) iron oxide, coated with 10 ± 3% (w/w) myristic acid, and stabilized by 16 ± 2% (w/w) Pluronic F127. TEM studies indicated that the mean Feret's diameter of the iron oxide core was 12 ± 3 nm

Table 1. SPIO NP Characterization

Composition	
form of iron oxide	magnetite
iron oxide content	74 ± 1.6%
myristic acid coating	10 ± 2.7%
Pluronic F127 coating	16 ± 1.6%
Particle Size	
particle size (TEM)	12 ± 3 nm
crystallite size (XRD)	12 ± 1 nm
hydrodynamic diameter (DLS)	185 nm
polydispersity	0.22
Magnetic Parameters	
saturation magnetization	60.5 emu/g magnetite
remanence	1.6 emu/g magnetite
coercivity	1.37 Oersted

(Figure 1A). This result was confirmed by the mean particle size calculated from XRD data (12 ± 1 nm) (Supporting Figure 2). SPIO NPs had an average hydrodynamic diameter of 185 nm, suggesting that particles in aqueous media existed as small aggregates rather than as individual SPIO NPs. FTIR spectroscopy showed the presence of characteristic magnetite bands at 570 cm^{-1} and 400 cm^{-1} and the absence of maghemite bands at 700 cm^{-1} and 630−660 cm^{-1}, indicating that the primary form of iron oxide in SPIO NPs was magnetite (data not shown).[26] SPIO NPs had a high saturation magnetization of 60.5 emu/g of magnetite, with negligible remanence and coercivity, verifying their superparamagnetic nature (Figure 1B). The heating rate of SPIO NPs was concentration-dependent and was similar in both cell culture medium and in agarose gel (Figure 1C,D). Based on the heating rates, a concentration of 2.5 mg/mL of SPIO NPs (equivalent to 1.85 mg/mL of magnetite) was found to be optimal for inducing magnetic hyperthermia *in vitro*.

Effect of Magnetic Hyperthermia on CSCs. *a. Side Population in A549 Cells.* The side population phenotype, characterized by overexpression of efflux transporters, is believed to be rich in CSCs.[19,20] Hoechst 33342 is a substrate of both P-glycoprotein (P-gp) and Breast Cancer Resistance Protein (BCRP), and the assay is therefore considered a direct correlate of transporter expression. The difference in the fraction of Hoechst 33342-negative cells with and without the dual efflux inhibitor tariquidar is considered the side population. Interestingly, magnetic hyperthermia resulted in a considerable decrease in the side population (~12% in magnetic hyperthermia group vs 20% in the nonhyperthermia SPIO NP control) (Figure 2A).

b. Mammosphere Assay. Mammospheres are clusters of mammary tumor cells growing in an anchorage-independent fashion and have been shown to be a quantitative indicator of the CSC subpopulation.[27] We observed a significant reduction ($P < 0.01$ vs untreated cells) in mammosphere formation in MDA-MB-231 cells following magnetic hyperthermia (Figure 2B). Untreated cells or cells subjected to conventional hyperthermia formed rigid mammospheres, whereas magnetic hyperthermia treated groups formed smaller spheres (Supporting Figure 3). While 5 and 15 min of magnetic hyperthermia resulted in 63% and 90% reduction in mammosphere formation, respectively, there was a complete absence of mammosphere formation after 30 min of magnetic hyperthermia.

c. ALDH Assay. High levels of ALDH have been reported for normal and cancer precursor cells.[22,25] To determine the effect of magnetic hyperthermia on cells with differential ALDH expression, MDA-MB-231 cells were sorted based on the overall levels of the ALDH enzyme. Clonogenicity studies revealed that both $ALDH_{high}$ and $ALDH_{low}$ cells were equally susceptible to magnetic hyperthermia, with a complete absence of colony formation following magnetic hyperthermia in either population

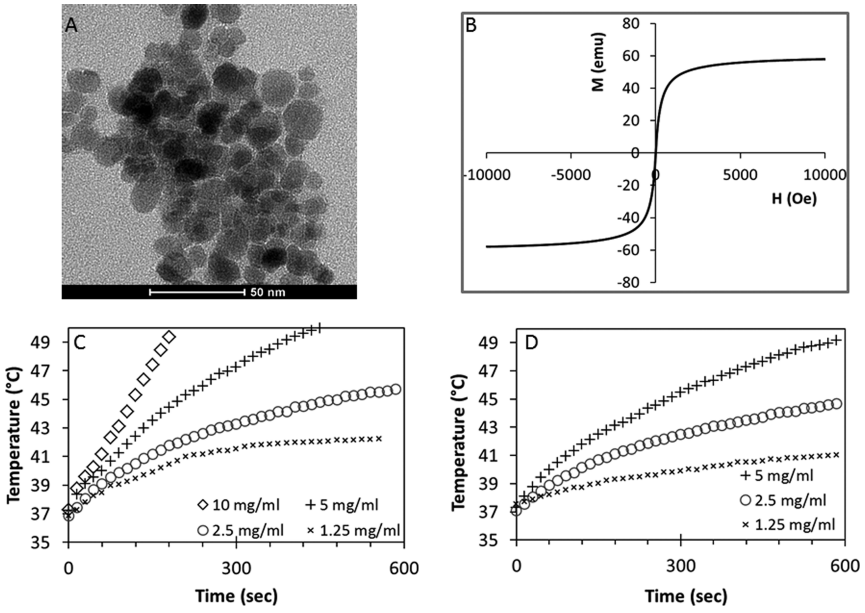

Figure 1. Characterization of SPIO NPs. (A) Representative TEM image of SPIO NPs. A drop of aqueous NP suspension was placed on a TEM grid and air-dried before observing under an electron microscope. Scale bar, 50 nm. (B) Magnetization. Magnetization curves were recorded on a vibrating sample magnetometer. The curve was normalized to the weight of magnetite added to obtain saturation magnetization per gram of magnetite. The sigmoidal curve is characteristic of superparamagnetic substances. Heating rates of SPIO NPs dispersed in (C) cell culture medium and (D) agarose gel. SPIO NP dispersions in a borosilicate glass tube were placed in an alternating magnetic field of 6 kA/m and operating at a frequency of 386 kHz. The initial temperature was equilibrated to 37 °C, and the temperature of SPIO NP dispersion was sampled at 15 s intervals using a fluoroptic probe following the application of the alternating magnetic field.

dx.doi.org/10.1021/mp400015b | *Mol. Pharmaceutics* 2013, 10, 1432−1441

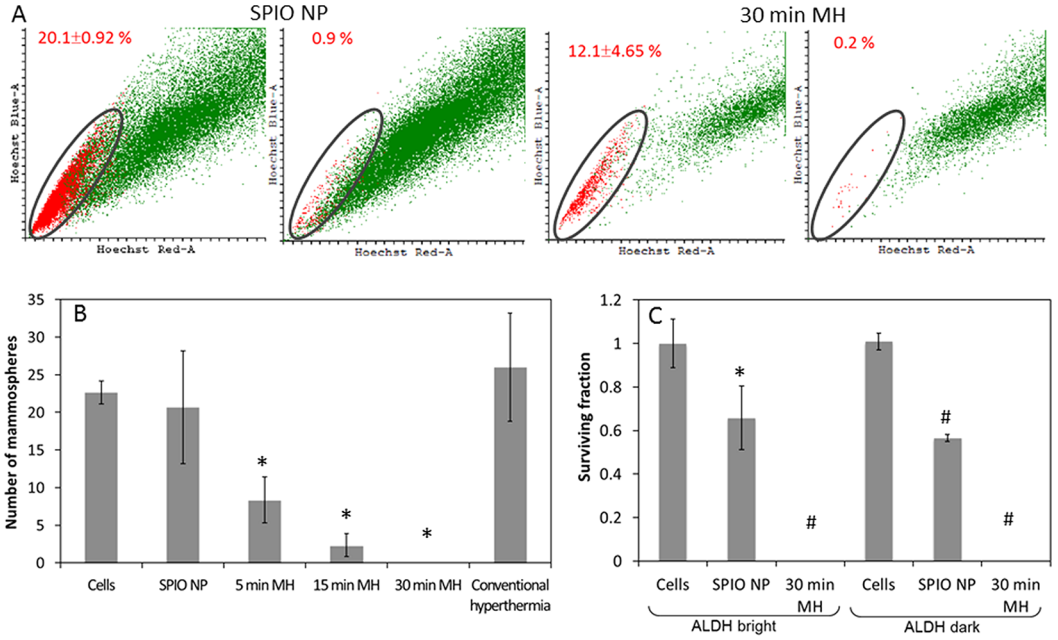

Figure 2. Effect of magnetic hyperthermia on CSCs. (A) Side population assay. Following magnetic hyperthermia, A549 cells were incubated with Hoechst 33342 dye at 37 °C for 90 min followed by flow cytometric analysis of Hoechst 33342 fluorescence in blue and red channels. Cells pretreated with tariquidar (a dual P-gp and BCRP efflux inhibitor) were used as controls. The flow images shown are representative Hoechst profiles of cells treated with SPIO NPS with (right) and without (left) heating. Side population is shown circumscribed within the oval area. The average percent (±S.D.) of side population is shown for each group, $n = 3$. (B) Mammosphere formation. After magnetic hyperthermia, 3000 live cells (counted by trypan blue exclusion) were plated in ultralow adhesion 6-well plates with mammosphere medium and left undisturbed at 37 °C. The number of mammospheres formed was counted using a light microscope on day 5 after treatment. Data shown is mean ± S.D., $n = 3$. *$P < 0.01$ vs untreated cells. (C) Clonogenicity of $ALDH_{high}$ and $ALDH_{low}$ MDA-MB-231 cells. MDA-MB-231 cells were sorted based on ALDH enzyme levels and then subjected to 30 min of magnetic hyperthermia. Post-treatment, 200 live cells were plated for clonogenicity assessment. The graph shows the relative survival fraction compared to untreated cells. Data shown is mean ± S.D., $n = 3$. *$P < 0.05$; #$P < 0.001$ vs untreated cells.

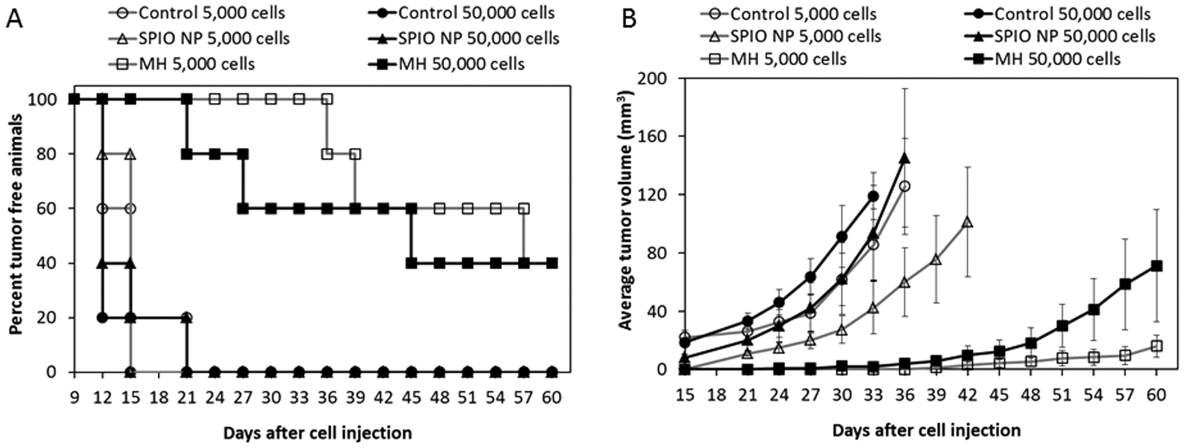

Figure 3. *In vivo* tumorigenicity of magnetic hyperthermia treated cells. A549 cells subjected to magnetic hyperthermia were injected subcutaneously into BALB-nude mice at a cell density of 5000 or 50 000 live cells per animal. Untreated cells or cells incubated with SPIO NPs but not exposed to alternating magnetic field were used as controls. A tumor size of 100 mm^3 or 60 days post cell injection (whichever came first) marked the end of the study. (A) Percent tumor-free animals and (B) average tumor volumes plotted as a function of days after cell injection. Data shown is mean ± S.D., $n = 5$.

(Figure 2C). Treatment with SPIO NP also caused a smaller but significant ($p < 0.05$) reduction in clonogenicity of both $ALDH_{high}$ and $ALDH_{low}$ cells.

d. Tumorigenicity Assay. A characteristic feature of CSCs is their ability to initiate a tumor in xenotransplantation assays.[28] *In vivo* tumor initiation study performed in nude mice showed a significant delay in tumor initiation with magnetic hyperthermia-treated cells compared to the corresponding controls. While most control animals developed a tumor within 15 days of cell injection, the first tumor appeared in magnetic hyperthermia-treated groups at 21 days (50 000 cell injection) or 36 days (5000 cell injection) postinjection (Figure 3A). Furthermore, 40% of the animals that received magnetic hyperthermia-treated tumor cells did not develop tumors even at 60 days post cell injection (Figure 3B).

Cell Kill after Magnetic Hyperthermia. LDH released by cells was used as a quantitative indicator of cell death.[29] Magnetic hyperthermia effectively induced cell death in both A549 and MDA-MB-231 cells (Figure 4A), and the efficacy of cell kill was found to increase with increasing duration of exposure to

dx.doi.org/10.1021/mp400015b | *Mol. Pharmaceutics* 2013, 10, 1432−1441

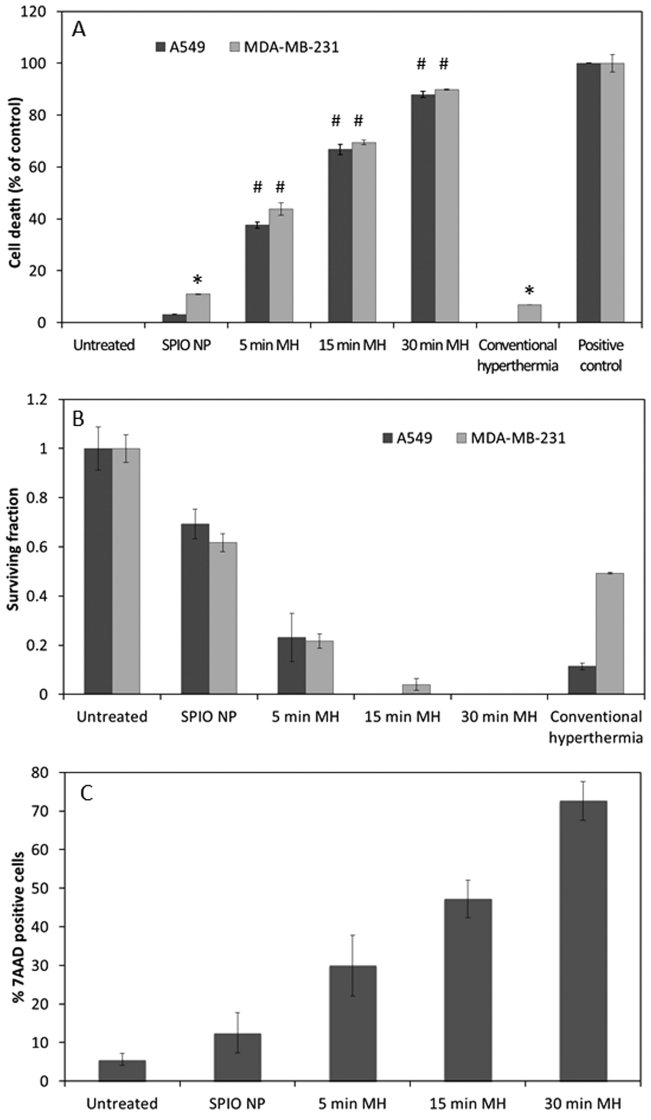

Figure 4. Effect of magnetic hyperthermia on A549 tumor cell kill. (A) LDH release. Cells were subjected to magnetic hyperthermia for 5, 15, or 30 min, following which the supernatant medium was assayed for the amount of LDH released after 2 h of treatment. SPIO NP-treated cells (without exposure to AMF) and cells subjected to 30 min of conventional hyperthermia at 46 °C were used as controls. Equal numbers of freeze−thaw lysed cells were used to determine LDH release from 100% cell death while untreated cells were used to determine background LDH release. Data shown is mean ± S.D., $n = 3$. *$P < 0.05$; #$P < 0.01$ vs untreated cells. (B) Clonogenicity. About 200 live cells from each treatment group were plated in a 10 cm tissue culture plate and observed for colony formation. The number of colonies formed was counted 2 weeks later. Data shown is mean ± S.D., $n = 3$. All treatments resulted in statistical significant ($P < 0.01$) decrease in surviving fraction. (C) Instantaneous 7AAD uptake. 7AAD was added to each treatment tube immediately prior to magnetic hyperthermia. After treatment, the cells were washed to eliminate excess 7AAD and subjected to flow cytometric analysis. Data shown is mean ± S.D., $n = 3$. All hyperthermia treatments resulted in statistical significant ($P < 0.01$) increase in 7AAD uptake.

magnetic hyperthermia. Prolonged (30 min) treatment resulted in 88% and 90% cell death in A549 and MDA-MB-231 cells, respectively. Conventional hyperthermia for 30 min was much less effective in killing cancer cells compared to magnetic hyperthermia.

Induction of apoptosis after magnetic hyperthermia was determined in the cells that survived after a recovery period of 10 h after treatment (about 10% in 30 min treatment group). The overall percent of healthy cells decreased with increasing duration of treatment (Table 2). The proportion of early apoptotic cells was higher for 5 and 15 min magnetic hyperthermia but was lower for 30 min treatment compared to SPIO NP-treated cells. However, there was a higher percent of late apoptotic/necrotic cells in the group exposed to 30 min of magnetic hyperthermia. Conventional hyperthermia was much less effective than magnetic hyperthermia in inducing apoptosis (2% early apoptotic cells and 6% late apoptotic cells).

Table 2. Induction of Apoptosis and Necrosis in A549 Cells Determined by Annexin-V/PI Assay

	(PI−/A−) (healthy)	(PI−/A+) (early apoptotic)	(PI+/A+) (late apoptotic)	(PI+/A−) (necrotic)
untreated cells	97	1	1	0.4
SPIO NP	97	0.6	2	0.7
5 min magnetic hyperthermia	92	2	6	0.4
15 min magnetic hyperthermia	81	3	14	2
30 min magnetic hyperthermia	62	2	33	3
conventional hyperthermia	93	2	6	0.2

A clonogenicity assay showed that magnetic hyperthermia resulted in a decrease in the proliferative ability and survival of both A549 and MDA-MB-231 cells (Figure 4B). Notably, cells subjected to 30 min of magnetic hyperthermia did not form any colonies in either cell line.

Instantaneous 7AAD uptake was used as a measure of acute cell kill during magnetic hyperthermia. As can be seen from Figure 4c, magnetic hyperthermia induced instantaneous 7AAD uptake in the treated cells. The 7AAD profile (30%, 47%, and 73% after 5 min, 15 min, and 30 min of magnetic hyperthermia, respectively) was comparable to the LDH profile (Figure 4A). No significant 7AAD uptake was observed in cells exposed to conventional hyperthermia.

ROS Generation during Magnetic Hyperthermia. ROS generation increased with increased duration of magnetic hyperthermia (Figure 5A). Conventional hyperthermia did not affect ROS levels compared to untreated cells. Following magnetic hyperthermia, ROS positive population appeared to become necrotic with time, as evidenced by the migration of ROS^{high}/PI^{low} population to the ROS^{high}/PI^{high} quadrant (Figure 5B). The addition of *N*-acetyl cysteine, an antioxidant,[30] inhibited ROS generation (not shown) and decreased the fraction of cells becoming PI positive without affecting the initial population of cells that took up PI instantaneously (Figure 5C). Interestingly, though ROS production and PI uptake by cells that underwent conventional hyperthermia was comparable to that by untreated cells, cells subjected to conventional hyperthermia in the presence of SPIO NPs demonstrated greater ROS production compared to those that received only SPIO NPs (Supporting Figure 4).

DISCUSSION

Magnetic hyperthermia, a technique involving the use of SPIO NPs subjected to AMF to generate heat,[13] has been studied for treating tumors as early as 1957.[31] The main advantage of

dx.doi.org/10.1021/mp400015b | Mol. Pharmaceutics 2013, 10, 1432−1441

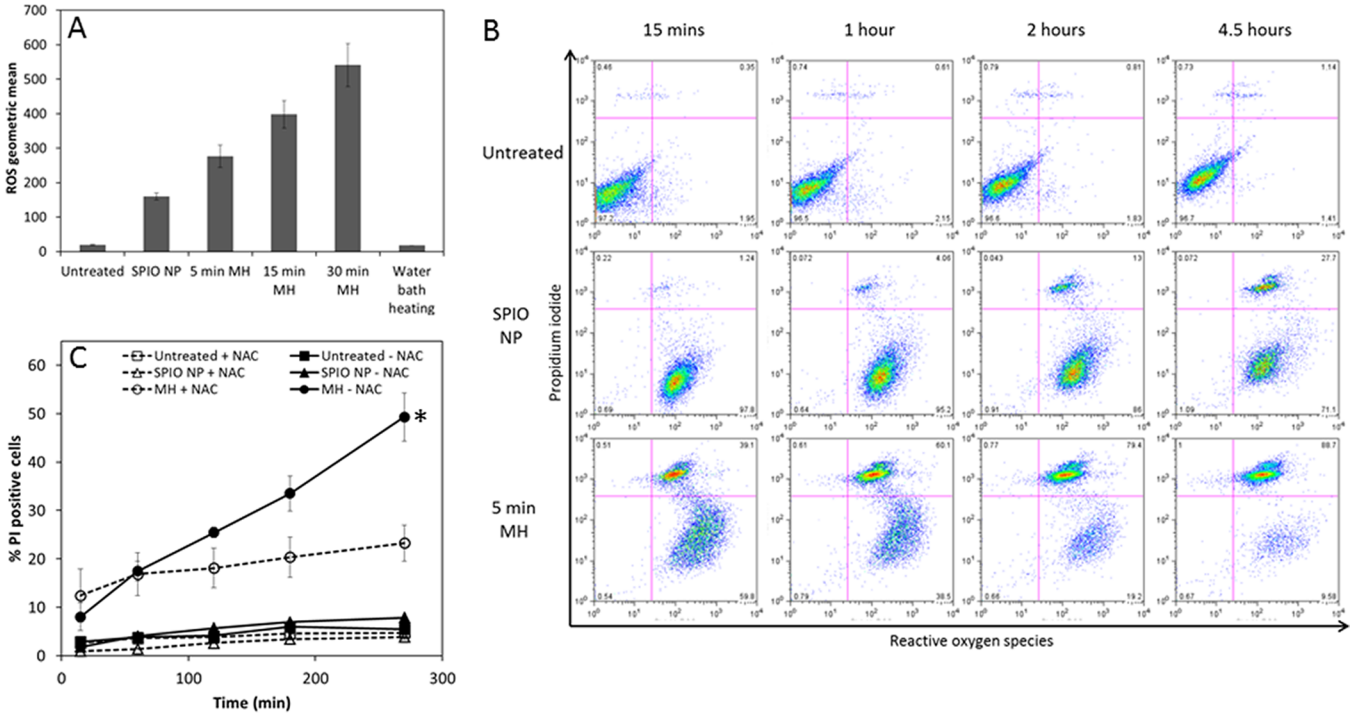

Figure 5. Effect of magnetic hyperthermia on ROS generation. (A) ROS generation immediately after treatment. CM-H_2DCFDA was added to A549 cells immediately before exposure to alternating magnetic field, followed by flow cytometric analysis to determine ROS levels. The graph shows the effect of treatments on geometric mean intensity of fluorescence, an indicator of ROS levels in the cells. Data shown is mean ± S.D., $n = 3$. All treatments resulted in statistical significant ($P < 0.01$) increase in the geometric mean intensity of ROS fluorescence. (B) Kinetic study to monitor ROS levels and PI uptake by cells subjected to magnetic hyperthermia. Cells were first treated with CM- H_2DCFDA and PI and then subjected to 5 min of magnetic hyperthermia. Fluorescence from ROS generation and PI uptake by the cells were monitored by flow cytometry. The change in the flow profile of untreated (top), cells treated with SPIO NPs (middle), and cells treated with magnetic hyperthermia (bottom) are shown at different times after treatment. (C) Effect of ROS scavenging on PI uptake by magnetic hyperthermia treated cells. Prior to SPIO NP or CM-H_2DCFDA addition and exposure to alternating magnetic field, cells were pretreated with *N*-acetyl cysteine (NAC) to scavenge free radicals. The percent of PI positive cells at different time point are plotted for the treatment groups. Data shown is mean ± S.D., $n = 3$. *$P < 0.001$ vs all other groups.

magnetic hyperthermia is that the heating rate can be well-controlled by adjusting particle size and shape of SPIO NPs as well as by modulating the properties of the alternating magnetic field.[32] There are several magnetic materials that can be used for inducing magnetic hyperthermia. However, most studies have focused on magnetic iron oxides, Fe_3O_4 (magnetite)[33] and γ-Fe_2O_3 (maghemite),[34] which have been proved to be well tolerated in clinical studies.[35] The core size of SPIO NPs dictates the primary mechanism of heat generation—Brownian relaxation and/or Néel relaxation.[36,37] The predominant mechanism of heat generation by 12 nm SPIO NPs used in our studies is through Néel relaxation, a mechanism of heat generation unaffected by suspending medium viscosity or by particle aggregation. This was confirmed from the similar heating rates observed for SPIO NPs in liquid and gel media. This data suggests that heat production by these particles will not likely be affected by the presence of dense extracellular matrix found in solid tumors.[38] Additionally, higher saturation magnetization of magnetic substances is more desirable, because this translates to higher heating rate per unit mass. SPIO NPs used in our studies were composed of magnetite, which possesses higher saturation magnetization than maghemite.[39] Optimum size and properties of synthesized SPIO NPs, along with their high saturation magnetization and iron content, allowed for effective induction of magnetic hyperthermia in our studies.

A number of preclinical studies have demonstrated the potential use of magnetic hyperthermia as an effective anticancer treatment modality.[13] In addition, magnetic hyperthermia is in clinical trials for different cancers.[14,40] However, there are no reports on the effect of magnetic hyperthermia on CSCs, a subpopulation that is thought to be responsible for tumor drug resistance and relapse.[41] Since no single assay is confirmatory with regard to the effect of treatments on CSCs, we evaluated the effect of magnetic hyperthermia on multiple biomarkers and functional properties of CSCs. Hoechst 33342 efflux[19] and ALDH[42] assays are functional assays identifying CSC-rich population, while mammosphere formation and tumorigenicity assays are based on the growth and proliferative properties unique to CSCs.[43] All of these assays indicated that magnetic hyperthermia reduced or, in some cases, eliminated the CSC subpopulation in treated cells.

Magnetic hyperthermia was effective in reducing CSC population in both long-term assays such as mammosphere formation as well as in short-term studies such as side population assay. The short-term effects of magnetic hyperthermia could be attributed to the induction of acute cell death, which was evident from high LDH release immediately after the treatment. The increased number of 7AAD positive cells immediately after treatment further points to the possibility of acute necrosis induced by magnetic hyperthermia. Lack of significant acute cell kill with conventional hyperthermia suggests that necrosis brought about by magnetic hyperthermia was likely temperature-independent. CSCs have been shown to be resistant to induction of apoptosis,[44] a slow programmed process of cell death. Necrosis is a more violent and acute cell death, most often mediated by mechanical damage to cell membrane and/or other

dx.doi.org/10.1021/mp400015b | *Mol. Pharmaceutics* 2013, 10, 1432−1441

vital cellular organelles.[45] If magnetic hyperthermia indeed caused necrosis, it is unlikely that CSCs will have resistance mechanisms to tolerate this acute cell death pathway.[28]

Exposure of cells to 30 min of magnetic hyperthermia resulted in the induction of apoptosis/necrosis in only about 35% of cells 12 h after treatment, suggesting that a majority of the cells are viable and healthy. However, these cells did not form any colonies in the clonogenicity assay. This implies that in addition to acute necrosis, there is a pronounced long-term effect of magnetic hyperthermia on CSCs. A mechanism postulated for the resistance of CSCs against DNA damage is decreased basal levels of ROS generation in CSCs.[6] Since SPIO NPs have been reported to induce ROS,[46] we investigated ROS generation as a possible mechanism of cell kill with magnetic hyperthermia. Immediately after magnetic hyperthermia, ROS levels were higher than in controls, and this appeared to be followed by a slow increase in the number of dying cells. Inhibition of ROS generation using an antioxidant suppressed this transition. These results suggest that magnetic hyperthermia induces ROS generation, which results in additional cell death after some latency. A similar increase in ROS production and cell death was observed in cells incubated with SPIO NPs and subjected to conventional hyperthermia but not in those subjected to either conventional hyperthermia alone or SPIO NP treatment alone. Overall, our studies suggest that ROS generation by magnetic hyperthermia is mediated by the presence of SPIO NPs and is amplified by higher temperatures. One possibility is that SPIO NPs generate ROS, which would normally be scavenged efficiently by CSCs;[47] however, generation of heat could decrease the ability of CSCs to scavenge ROS and thereby increases their susceptibility to ROS.

In our studies, all of the magnetic hyperthermia treatments were performed on suspended tumor cells. The size of the induction coil used prevented studies on plated cells. It is possible that suspended and adherent cells (either grown in two-dimensional plates or as three-dimensional spheres) may have different susceptibilities to magnetic hyperthermia. The effect of growth and plating conditions on the effect of magnetic hyperthermia on CSCs will be examined in our future studies.

CONCLUSIONS

CSCs are considered to play important roles in tumor drug resistance and recurrence. Our studies show that CSCs and non-CSCs are equally susceptible to cell death induced by magnetic hyperthermia. Further, magnetic hyperthermia induces both acute necrosis and a slower, ROS-mediated cell-death in treated cells. Some of the cell kill events appear to be temperature-independent, although elevated temperatures appear to amplify those effects. Overall, these results suggest the potential for effective CSC eradication by magnetic hyperthermia. Future studies will investigate the effect of magnetic hyperthermia on *in vivo* tumor growth and tumor recurrence.

ASSOCIATED CONTENT

Supporting Information

Temperature profile during magnetic hyperthermia, XRD pattern of SPIO NP, representative picture of mammospheres formed, and the PI positive population and geometric mean of ROS produced by the different treatment. This material is available free of charge via the Internet at http://pubs.acs.org.

AUTHOR INFORMATION

Corresponding Author

*Department of Pharmaceutics, College of Pharmacy, University of Minnesota, 308 Harvard St. SE, Minneapolis, MN 55455. Phone: 612-624-0951. Fax: 612-626-2125. E-mail: jpanyam@umn.edu.

Notes

The authors declare no competing financial interest.

ACKNOWLEDGMENTS

We thank the Flow Cytometry Core Facility of the Masonic Cancer Center, a comprehensive cancer center designated by the National Cancer Institute, supported in part by P30 CA77598. Parts of this work were carried out in the Characterization Facility, University of Minnesota, which receives partial support from NSF through the MRSEC program. We thank Dr. Nisha V. Shah (Flow Cytometry Core Facility, University of Minnesota) for assistance with side population studies, Dr. Robert S. Hafner (Characterization Facility, University of Minnesota) for help with TEM studies, Ying Jing (Electrical and Computer Engineering, University of Minnesota) for help with magnetization studies and Brenda Koniar (Research Animal Resources, University of Minnesota) for assistance with animal studies. Funding support from the Department of Defense (CA093453) is also acknowledged.

ABBREVIATIONS

7AAD,7-aminoactinomycin D; ALDH,aldehyde dehydrogenase; CM-H_2DCFDA,5-(and-6)-chloromethyl-2′,7′-dichlorodihydrofluorescein diacetate, acetyl ester; CSC,cancer stem cells; DPBS,Dulbecco's phosphate-buffered saline; FBS,fetal bovine serum; FT-IR,Fourier-transformed infrared spectroscopy; LDH,lactate dehydrogenase; PI,propidium iodide; ROS,reactive oxygen species; SPIO NP,superparamagnetic iron oxide nanoparticles; TEM,transmission electron microscopy

REFERENCES

(1) Chandler, J. M.; Lagasse, E. Cancerous stem cells: deviant stem cells with cancer-causing misbehavior. *Stem Cell Res. Ther.* **2010**, *1* (2), 13.

(2) Potten, C. S.; Loeffler, M. Stem cells: attributes, cycles, spirals, pitfalls and uncertainties. Lessons for and from the crypt. *Development* **1990**, *110* (4), 1001−1020.

(3) Li, X.; Lewis, M. T.; Huang, J.; Gutierrez, C.; Osborne, C. K.; Wu, M. F.; Hilsenbeck, S. G.; Pavlick, A.; Zhang, X.; Chamness, G. C.; Wong, H.; Rosen, J.; Chang, J. C. Intrinsic resistance of tumorigenic breast cancer cells to chemotherapy. *J. Natl. Cancer Inst.* **2008**, *100* (9), 672−9.

(4) Moitra, K.; Lou, H.; Dean, M. Multidrug efflux pumps and cancer stem cells: insights into multidrug resistance and therapeutic development. *Clin. Pharmacol. Ther.* **2011**, *89* (4), 491−502.

(5) Bao, S.; Wu, Q.; McLendon, R. E.; Hao, Y.; Shi, Q.; Hjelmeland, A. B.; Dewhirst, M. W.; Bigner, D. D.; Rich, J. N. Glioma stem cells promote radioresistance by preferential activation of the DNA damage response. *Nature* **2006**, *444* (7120), 756−760.

(6) Diehn, M.; Cho, R. W.; Lobo, N. A.; Kalisky, T.; Dorie, M. J.; Kulp, A. N.; Qian, D.; Lam, J. S.; Ailles, L. E.; Wong, M.; Joshua, B.; Kaplan, M. J.; Wapnir, I.; Dirbas, F. M.; Somlo, G.; Garberoglio, C.; Paz, B.; Shen, J.; Lau, S. K.; Quake, S. R.; Brown, J. M.; Weissman, I. L.; Clarke, M. F. Association of reactive oxygen species levels and radioresistance in cancer stem cells. *Nature* **2009**, *458* (7239), 780−3.

(7) Moore, N.; Lyle, S., Quiescent, slow-cycling stem cell populations in cancer: a review of the evidence and discussion of significance. *J. Oncol.* **2011**, *2011*.

(8) Dylla, S. J.; Beviglia, L.; Park, I. K.; Chartier, C.; Raval, J.; Ngan, L.; Pickell, K.; Aguilar, J.; Lazetic, S.; Smith-Berdan, S.; Clarke, M. F.; Hoey, T.; Lewicki, J.; Gurney, A. L. Colorectal cancer stem cells are enriched in xenogeneic tumors following chemotherapy. *PLoS One* **2008**, *3* (6), e2428.
(9) Dewhirst, M. W.; Prosnitz, L.; Thrall, D.; Prescott, D.; Clegg, S.; Charles, C.; MacFall, J.; Rosner, G.; Samulski, T.; Gillette, E.; LaRue, S. Hyperthermic treatment of malignant diseases: current status and a view toward the future. *Semin. Oncol.* **1997**, *24* (6), 616−25.
(10) Cotte, E.; Glehen, O.; Mohamed, F.; Lamy, F.; Falandry, C.; Golfier, F.; Gilly, F. N. Cytoreductive surgery and intraperitoneal chemo-hyperthermia for chemo-resistant and recurrent advanced epithelial ovarian cancer: prospective study of 81 patients. *World J. Surg.* **2007**, *31* (9), 1813−20.
(11) van der Zee, J.; Gonzalez Gonzalez, D.; van Rhoon, G. C.; van Dijk, J. D.; van Putten, W. L.; Hart, A. A. Comparison of radiotherapy alone with radiotherapy plus hyperthermia in locally advanced pelvic tumours: a prospective, randomised, multicentre trial. Dutch Deep Hyperthermia Group. *Lancet* **2000**, *355* (9210), 1119−25.
(12) Atkinson, R. L.; Zhang, M.; Diagaradjane, P.; Peddibhotla, S.; Contreras, A.; Hilsenbeck, S. G.; Woodward, W. A.; Krishnan, S.; Chang, J. C.; Rosen, J. M. Thermal enhancement with optically activated gold nanoshells sensitizes breast cancer stem cells to radiation therapy. *Sci. Transl. Med.* **2010**, *2* (55), 55ra79.
(13) Tseng, H. Y.; Lee, G. B.; Lee, C. Y.; Shih, Y. H.; Lin, X. Z. Localised heating of tumours utilising injectable magnetic nanoparticles for hyperthermia cancer therapy. *IET Nanobiotechnol.* **2009**, *3* (2), 46−54.
(14) Maier-Hauff, K.; Ulrich, F.; Nestler, D.; Niehoff, H.; Wust, P.; Thiesen, B.; Orawa, H.; Budach, V.; Jordan, A. Efficacy and safety of intratumoral thermotherapy using magnetic iron-oxide nanoparticles combined with external beam radiotherapy on patients with recurrent glioblastoma multiforme. *J. Neurooncol.* **2011**, *103* (2), 317−24.
(15) (a) Johannsen, M.; Thiesen, B.; Jordan, A.; Taymoorian, K.; Gneveckow, U.; Waldofner, N.; Scholz, R.; Koch, M.; Lein, M.; Jung, K.; Loening, S. A. Magnetic fluid hyperthermia (MFH)reduces prostate cancer growth in the orthotopic Dunning R3327 rat model. *Prostate* **2005**, *64* (3), 283−92. (b) Jones, S. K.; Winter, J. G.; Gray, B. N. Treatment of experimental rabbit liver tumours by selectively targeted hyperthermia. *Int. J. Hyperthermia* **2002**, *18* (2), 117−28. (c) Jordan, A.; Scholz, R.; Maier-Hauff, K.; van Landeghem, F. K.; Waldoefner, N.; Teichgraeber, U.; Pinkernelle, J.; Bruhn, H.; Neumann, F.; Thiesen, B.; von Deimling, A.; Felix, R. The effect of thermotherapy using magnetic nanoparticles on rat malignant glioma. *J. Neurooncol.* **2006**, *78* (1), 7−14. (d) Balivada, S.; Rachakatla, R. S.; Wang, H.; Samarakoon, T. N.; Dani, R. K.; Pyle, M.; Kroh, F. O.; Walker, B.; Leaym, X.; Koper, O. B.; Tamura, M.; Chikan, V.; Bossmann, S. H.; Troyer, D. L. A/C magnetic hyperthermia of melanoma mediated by iron(0)/iron oxide core/shell magnetic nanoparticles: a mouse study. *BMC Cancer* **2010**, *10*, 119.
(16) Jain, T. K.; Morales, M. A.; Sahoo, S. K.; Leslie-Pelecky, D. L.; Labhasetwar, V. Iron oxide nanoparticles for sustained delivery of anticancer agents. *Mol. Pharmaceutics* **2005**, *2* (3), 194−205.
(17) Tae-Youb, K.; Yamazaki, Y. Determination of the magnetic compensation composition in Al-substituted Bi-DyCoIG nanoparticles with enhanced coercive-force. *IEEE Trans. Magn.* **2004**, *40* (4), 2793−2795.
(18) Krishna Murti, G. S. R.; Moharir, A. V.; Sarma, V. A. K. Spectrophotometric determination of iron with orthophenanthroline. *Microchem. J.* **1970**, *15* (4), 585−589.
(19) Ho, M. M.; Ng, A. V.; Lam, S.; Hung, J. Y. Side population in human lung cancer cell lines and tumors is enriched with stem-like cancer cells. *Cancer Res.* **2007**, *67* (10), 4827−33.
(20) Sung, J.-M.; Cho, H.-J.; Yi, H.; Lee, C.-H.; Kim, H.-S.; Kim, D.-K.; Abd El-Aty, A. M.; Kim, J.-S.; Landowski, C. P.; Hediger, M. A.; Shin, H.-C. Characterization of a stem cell population in lung cancer A549 cells. *Biochem. Biophys. Res. Commun.* **2008**, *371* (1), 163−167.
(21) Grimshaw, M.; Cooper, L.; Papazisis, K.; Coleman, J.; Bohnenkamp, H.; Chiapero-Stanke, L.; Taylor-Papadimitriou, J.; Burchell, J. Mammosphere culture of metastatic breast cancer cells enriches for tumorigenic breast cancer cells. *Breast Cancer Res.* **2008**, *10* (3), R52.
(22) Ginestier, C.; Hur, M. H.; Charafe-Jauffret, E.; Monville, F.; Dutcher, J.; Brown, M.; Jacquemier, J.; Viens, P.; Kleer, C. G.; Liu, S.; Schott, A.; Hayes, D.; Birnbaum, D.; Wicha, M. S.; Dontu, G. ALDH1 is a marker of normal and malignant human mammary stem cells and a predictor of poor clinical outcome. *Cell Stem Cell* **2007**, *1* (5), 555−567.
(23) Franken, N. A. P.; Rodermond, H. M.; Stap, J.; Haveman, J.; van Bree, C. Clonogenic assay of cells in vitro. *Nat. Protocols* **2006**, *1* (5), 2315−2319.
(24) He, L.; Yang, C. P.; Horwitz, S. B. Mutations in beta-tubulin map to domains involved in regulation of microtubule stability in epothilone-resistant cell lines. *Mol. Cancer Ther.* **2001**, *1* (1), 3−10.
(25) Croker, A. K.; Goodale, D.; Chu, J.; Postenka, C.; Hedley, B. D.; Hess, D. A.; Allan, A. L. High aldehyde dehydrogenase and expression of cancer stem cell markers selects for breast cancer cells with enhanced malignant and metastatic ability. *J. Cell. Mol. Med.* **2009**, *13* (8B), 2236−52.
(26) Namduri, H.; Nasrazadani, S. Quantitative analysis of iron oxides using Fourier transform infrared spectrophotometry. *Corros. Sci.* **2008**, *50* (9), 2493−2497.
(27) Iliopoulos, D.; Hirsch, H. A.; Wang, G.; Struhl, K. Inducible formation of breast cancer stem cells and their dynamic equilibrium with non-stem cancer cells via IL6 secretion. *Proc. Natl. Acad. Sci. U.S.A.* **2011**, *108* (4), 1397−402.
(28) Burke, A. R.; Singh, R. N.; Carroll, D. L.; Wood, J. C. S.; D'Agostino, R. B., Jr.; Ajayan, P. M.; Torti, F. M.; Torti, S. V. The resistance of breast cancer stem cells to conventional hyperthermia and their sensitivity to nanoparticle-mediated photothermal therapy. *Biomaterials* **2012**, *33* (10), 2961−2970.
(29) Korzeniewski, C.; Callewaert, D. M. An enzyme-release assay for natural cytotoxicity. *J. Immunol. Methods* **1983**, *64* (3), 313−20.
(30) Spagnuolo, G.; D'Anto, V.; Cosentino, C.; Schmalz, G.; Schweikl, H.; Rengo, S. Effect of N-acetyl-L-cysteine on ROS production and cell death caused by HEMA in human primary gingival fibroblasts. *Biomaterials* **2006**, *27* (9), 1803−9.
(31) Gilchrist, R. K.; Medal, R.; Shorey, W. D.; Hanselman, R. C.; Parrott, J. C.; Taylor, C. B. Selective inductive heating of lymph nodes. *Ann. Surg.* **1957**, *146* (4), 596−606.
(32) Kalambur, V. S.; Han, B.; Hammer, B. E.; Shield, T. W.; Bischof, J. C. In vitro characterization of movement, heating and visualization of magnetic nanoparticles for biomedical application. *Nanotechnology* **2005**, *16*, 1221−33.
(33) (a) Wada, S.; Tazawa, K.; Furuta, I.; Nagae, H. Antitumor effect of new local hyperthermia using dextran magnetite complex in hamster tongue carcinoma. *Oral Dis.* **2003**, *9* (4), 218−23. (b) Liu, J.; Sun, Z.; Deng, Y.; Zou, Y.; Li, C.; Guo, X.; Xiong, L.; Gao, Y.; Li, F.; Zhao, D. Highly water-dispersible biocompatible magnetite particles with low cytotoxicity stabilized by citrate groups. *Angew. Chem., Int. Ed. Engl.* **2009**, *48* (32), 5875−9.
(34) (a) Schulze, K.; Koch, A.; Petri-Fink, A.; Steitz, B.; Kamau, S.; Hottiger, M.; Hilbe, M.; Vaughan, L.; Hofmann, M.; Hofmann, H.; von Rechenberg, B. Uptake and biocompatibility of functionalized poly-(vinylalcohol) coated superparamagnetic maghemite nanoparticles by synoviocytes in vitro. *J. Nanosci. Nanotechnol.* **2006**, *6* (9−10), 2829−40. (b) Halbreich, A.; Roger, J.; Pons, J. N.; Geldwerth, D.; Da Silva, M. F.; Roudier, M.; Bacri, J. C. Biomedical applications of maghemite ferrofluid. *Biochimie* **1998**, *80* (5−6), 379−90.
(35) Corot, C.; Robert, P.; Idee, J. M.; Port, M. Recent advances in iron oxide nanocrystal technology for medical imaging. *Adv. Drug Delivery Rev.* **2006**, *58* (14), 1471−504.
(36) Rosensweig, R. E. Heating magnetic fluid with alternating magnetic field. *J. Magn. Magn. Mater.* **2002**, *252* (0), 370−374.
(37) Hergt, R.; Andra, W.; d'Ambly, C. G.; Hilger, I.; Kaiser, W. A.; Richter, U.; Schmidt, H. G. Physical limits of hyperthermia using magnetite fine particles. *IEEE Trans. Magn.* **1998**, *34* (5), 3745−3754.
(38) Heldin, C. H.; Rubin, K.; Pietras, K.; Ostman, A. High interstitial fluid pressure—an obstacle in cancer therapy. *Nat. Rev. Cancer* **2004**, *4* (10), 806−13.

(39) Rebodos, R. L.; Vikesland, P. J. Effects of oxidation on the magnetization of nanoparticulate magnetite. *Langmuir* **2010**, *26* (22), 16745−53.
(40) http://www.magforce.de/english/clinical-trials/overview.html.
(41) Wehner, H.; von Ardenne, A.; Kaltofen, S. Whole-body hyperthermia with water-filtered infrared radiation: technical-physical aspects and clinical experiences. *Int. J. Hyperthermia* **2001**, *17* (1), 19−30.
(42) Issels, R. D.; Abdel-Rahman, S.; Wendtner, C.; Falk, M. H.; Kurze, V.; Sauer, H.; Aydemir, U.; Hiddemann, W. Neoadjuvant chemotherapy combined with regional hyperthermia (RHT) for locally advanced primary or recurrent high-risk adult soft-tissue sarcomas (STS) of adults: long-term results of a phase II study. *Eur. J. Cancer* **2001**, *37* (13), 1599−608.
(43) Charafe-Jauffret, E.; Ginestier, C.; Birnbaum, D. Breast cancer stem cells: tools and models to rely on. *BMC Cancer* **2009**, *9*, 202.
(44) Krakstad, C.; Chekenya, M. Survival signalling and apoptosis resistance in glioblastomas: opportunities for targeted therapeutics. *Mol. Cancer* **2010**, *9*, 135.
(45) Festjens, N.; Vanden Berghe, T.; Vandenabeele, P. Necrosis, a well-orchestrated form of cell demise: signalling cascades, important mediators and concomitant immune response. *Biochim. Biophys. Acta* **2006**, *1757* (9−10), 1371−87.
(46) Apopa, P. L.; Qian, Y.; Shao, R.; Guo, N. L.; Schwegler-Berry, D.; Pacurari, M.; Porter, D.; Shi, X.; Vallyathan, V.; Castranova, V.; Flynn, D. C. Iron oxide nanoparticles induce human microvascular endothelial cell permeability through reactive oxygen species production and microtubule remodeling. *Part. Fibre Toxicol.* **2009**, *6*, 1.
(47) Seton-Rogers, S. Cancer stem cells: Survival skills. *Nat. Rev. Cancer* **2009**, *9* (3), 147−147.